Anomalous behavior of a single particle falling through a funnel

Yuan Fang, Ming Gao, Jonathan J. Wylie, and Qiang Zhang
Department of Mathematics, City University of Hong Kong, Tat Chee Avenue, Kowloon, Hong Kong, China
(Received 16 August 2007; revised manuscript received 24 December 2007; published 3 April 2008)

We show several surprising phenomena that occur in an extremely simple system of a single frictionless, inelastic, spherical particle falling under gravity through a symmetric funnel. One might naively expect that particles would fall through funnels with steeper sides more quickly, exert a smaller total impulse on the funnel walls, and lose less energy. However, we show that there are special ranges of angles of the funnel walls for which exactly the opposite occurs. Typically, the particle will experience a sequence of collisions that is highly sensitive to the location at which it enters the funnel and nearby particle trajectories become widely dispersed. However, in the special angular ranges this is not the case and the particle can experience sequences of collisions that have a highly coherent structure. We provide a theoretical analysis that can predict and explain this surprising behavior.

DOI: 10.1103/PhysRevE.77.041302 PACS number(s): 81.05.Rm, 45.50.−j

I. INTRODUCTION

There are a broad range of industrial applications in which particles fall under gravity and interact inelastically with rigid boundaries. In many applications devices are designed to take falling particles and guide them into a thin slot or hole. We consider an extremely simple example of a single inelastic particle falling under gravity through a symmetric funnel. Despite the simplicity of the system we show that surprising dynamics can occur for funnels whose walls are inclined at certain angles.

In applications there are a number of objectives that such devices may be required to achieve. These include reducing the speed of particles exiting the machine or minimizing the time that particles spend in the device so that interactions with other particles and jamming are less likely. Details of the particle trajectories and the impulses experienced by such devices are critical for understanding how these objectives can be best achieved. This knowledge is also required to develop strategies for minimizing excessive wear on devices.

Flows with large numbers of particles in funnels have been widely studied and a number of important results have been obtained [1–10]. A wide range of work has been done that includes cases in which the stresses are dominated by frictional forces and cases in which the stresses are dominated by interparticle collisions [11]. However, despite its obvious importance in many applications, the case of a single particle falling through a hopper has received much less attention.

Systems that contain only a single particle or a small number of particles appear to be extremely simple, but can contain surprisingly subtle and complex dynamics. Studies of this type of system have led to important insights into the way in which granular materials behave. Mehta and Luck [12] and Luck and Mehta [13] showed that a single particle moving under gravity on a vibrating plate can give rise to highly unexpected behavior, such as abrupt termination of period-doubling sequences. McNamara and Young [14] showed that a finite number of particles is required to obtain an infinite number of collisions in a finite time. Wylie and Zhang [15] have shown that two driven inelastic particles can experience a bifurcation in which large numbers of complicated periodic orbits collapse onto a single simple orbit.

II. FORMULATION

In this paper, we consider a frictionless, inelastic particle of radius a falling under gravity g through a symmetric funnel with walls aligned at an angle θ to the horizontal and a gap of size d at the bottom of the funnel. The particle is released with zero initial velocity with its center at a height H above the bottom of the funnel and at a horizontal location x_0 measured from the central axis of the funnel (see Fig. 1). When the particle collides with the walls it experiences an inelastic collision with coefficient of restitution e. Here e is defined as the ratio of the velocity normal to the wall immediately after to that immediately before the collision.

We will consider the case where particles are dropped into the funnel at a random horizontal location x_0. For simplicity we consider the distribution in which all locations have uniform probability of being chosen. Other distributions yield similar behavior. We note that the dynamics of the particle are identical for both a two-dimensional funnel and a radially

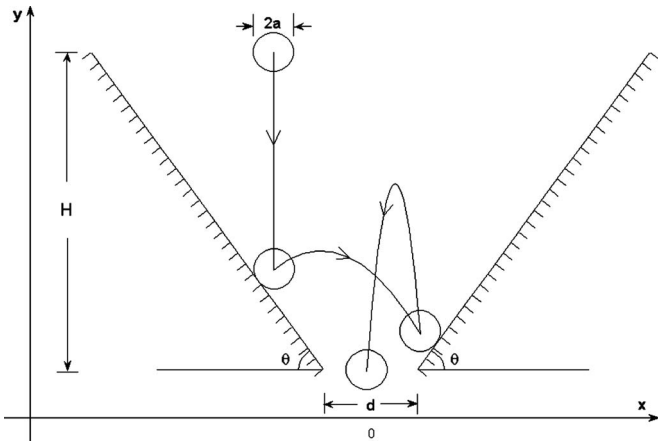

FIG. 1. Sketch of a system in which a particle falls through a funnel with an angle θ.

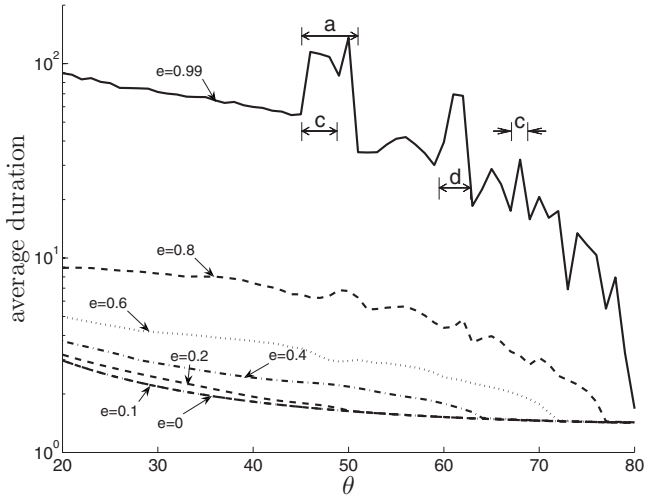

FIG. 2. The average duration is plotted against θ for different values of e. This shows that the average duration can be a nonmonotonic function of θ.

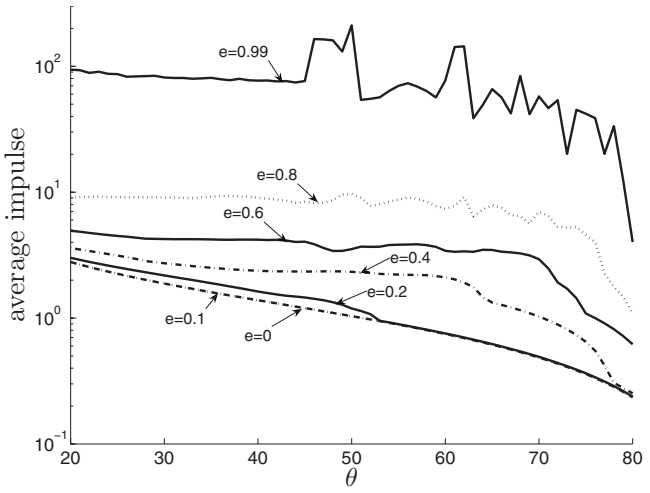

FIG. 3. The average impulse is plotted against θ for different values of e. The average impulse can be a nonmonotonic function of θ.

symmetric funnel. We nondimensionalize lengths by H, times by $\sqrt{H/g}$, and velocities by $\sqrt{Hg}$. In this paper, we will focus on the effects of inelasticity e and funnel angle θ.

The particle trajectory is composed of parabolic segments punctuated by collisions with the funnel walls. Each parabolic segment of the trajectory ends in one of three possible events: the particle collides with the left funnel wall, collides with the right funnel wall, or exits the funnel through the gap. The process of determining which of the three events occur leads to the very complicated nonlinear dynamics of this system. The implementation of numerical simulations of this complicated system is quite straightforward. When the event corresponds to a collision with one of the walls, the particle velocity is updated by performing an inelastic collision with the wall and the procedure is repeated until the particle exits the funnel. The phenomenon of inelastic collapse may occur, in which the particle may experience an infinite number of collisions with one of the walls in a finite time. This is easy to handle in simulations since the time of inelastic collapse can be determined analytically. After the collapse the particle will simply slide down the wall.

III. RESULTS

In our simulations, we choose $H=g=1$, $a=0.01$, and $d=0.04$. For given values of e and θ, we simulate 4000 sample trajectories with uniformly spaced initial horizontal locations x_0. For each x_0, we record the locations and the velocities of the particle when collisions occur. Using this information, it is straightforward to compute quantities such as the duration that the particle stays in the funnel, $\tau(x_0)$; the energy loss as the particle falls through the funnel; and the total impulse exerted by the particle on the funnel walls. In Fig. 2, we show the time that the particle stays in the funnel averaged over the horizontal release position as a function of θ for different values of e. Intuitively, one would expect that steeper funnels (i.e., larger values of θ) would lead to the particle, on average, spending less time in the funnel. However, this is only the case when $e<0.51\ldots$. For larger values of e, there are ranges of θ in which the particle will, on average, stay longer in a steeper funnel. This is clearly demonstrated for $e=0.8$ and 0.99 in Fig. 2 where the particle stays significantly longer in a funnel with $\theta=46°$ than a funnel with $\theta=45°$. This seems highly counterintuitive, and we will analyze theoretically why these specific angular ranges have this property.

In industrial applications, the impulse exerted on the walls is an important quantity for understanding machine wear. In computing the impulse, one must include the contribution after inelastic collapse when the particle slides down the wall. In Fig. 3, we show the average impulse as a function of θ for different values of e. Figure 3 shows that the behavior for the average total impulse is very similar to the behavior for the average duration shown in Fig. 2. That is, a steeper funnel can experience a larger average total impulse than a less steep funnel.

When the particle collides with the funnel boundaries, it loses energy. Figure 4 shows the average energy loss when

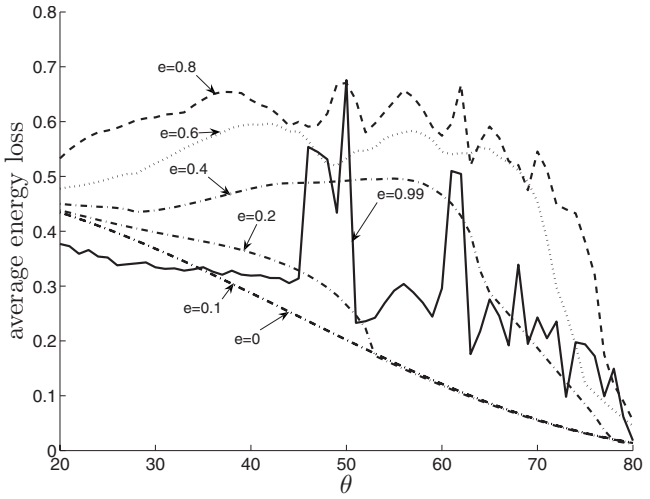

FIG. 4. The average energy loss is plotted against θ for different values of e.

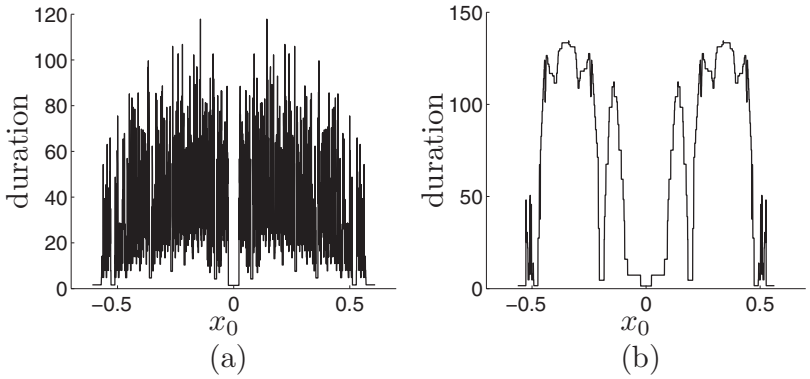

FIG. 5. The duration is plotted against the initial location x_0 for $e=0.99$ and funnels with (a) $\theta=59°$ and (b) $\theta=61°$. The behavior in (a) and (b) is completely different even though the change in θ is very small.

the particle exits the funnel. It reveals several interesting phenomena. First, for e close to unity, there are sudden jumps in the average energy loss as θ varies. The angles θ at which these jumps occur coincide with those observed in Fig. 2 and 3. We will explain the cause of these jumps later. Second, one might naively expect that, on average, a particle with smaller e would lose more energy than the one with larger e. However, Fig. 4 shows that the energy loss is not a monotonic function of e. The curve for $e=0.8$ has higher energy loss than the curves for other values of e shown. This is due to the fact that both energy loss per collision and number of collisions contribute to the energy loss. The contribution from the first factor is a monotonic function of e, but the combined effects from both factors are not. Third, for $e \leq 0.1$, all curves almost coincide. When $e \ll 1$, the particle will typically experience rapid collisions with only one of the funnel walls before exiting the funnel. When the particle only collides with one of the walls the velocity component parallel to that wall is unaffected by collisions, whereas the component perpendicular to the wall will be damped by rapid collisions. So the remaining energy is dominated by the velocity component parallel to the boundary which is independent of e when e is sufficiently small. This is in contrast to the case where the particle collides with both boundaries. In this case, the two different boundaries have different normal vectors and so change the components of velocity in different directions. Furthermore, the velocity component perpendicular to the boundary is a monotonic decreasing function of θ. Therefore the energy loss is a monotonic decreasing function of θ when $e \ll 1$. Fourth, as θ approaches 90°, few collisions will occur. Therefore the energy loss approaches zero for all values of e when θ approaches 90°.

Now we examine the sudden jumps in duration and energy loss. These jumps can clearly be seen in Figs. 2–4 as θ changes from 45° to 46° and from 59° to 61°. To investigate these dramatic changes, we compare the duration spent in the funnel as a function of the input location x_0 in funnels with $\theta=59°$ [Fig. 5(a)] and $\theta=61°$ [Fig. 5(b)]. In both Figs. 5(a) and 5(b), $e=0.99$. Despite the small difference in θ, the behavior is completely different. For $\theta=59°$, the duration is highly sensitive to initial location whereas for $\theta=61°$ the duration is extremely robust and there are wide ranges of injection locations where the duration remains almost constant.

We now examine the typical trajectories that occur in funnels with $\theta=59°$ and $\theta=61°$ in Fig. 6. The particle loses energy during collisions, and so the collision locations have a tendency of moving downwards toward the exit. This is true for both funnel angles shown in Figs. 6(a) and 6(b). However, for $\theta=61°$ [Fig. 6(b)] the particle experiences a very coherent sequence of collisions with a simple repeating pattern. After each pattern the trajectory remains relatively tightly confined and the collision locations move slowly downward toward the exit. During the bulk of the trajectory the collision points are not near the exit. This means that the particle experiences a relatively large number of collisions, loses a large amount of energy, and takes a long time to exit the funnel. In contrast, for $\theta=59°$ [Fig. 6(a)] the particle follows a trajectory with no clear pattern of collisions. The locations of collisions are widely dispersed throughout the funnel. Consequently, there is a larger probability of the particle falling through the funnel exit after a relatively small number of collisions and in a relatively short time. The energy loss will also be comparably small. This gives a qualitative explanation of the phenomenon of sudden jumps in the average duration, average impulse, and the average energy loss shown in Figs. 2–4. In Sec. IV we give a theoretical prediction about the locations of these jumps.

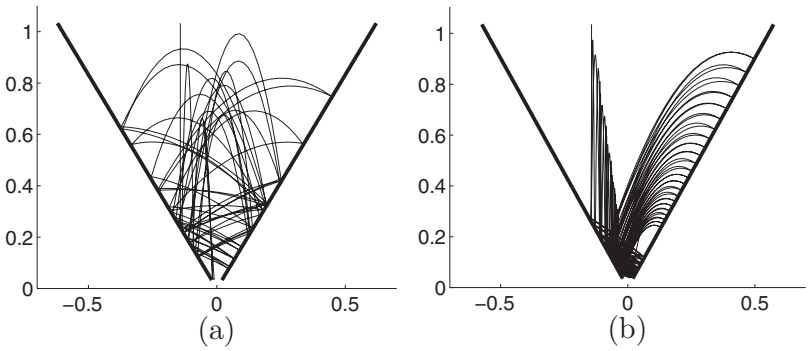

FIG. 6. Some typical particle trajectories for $e=0.99$ and funnels with (a) $\theta=59°$ and (b) $\theta=61°$. In both cases, the initial horizontal location is $x_0=-0.14$. There is no coherent pattern of collisions in (a), but (b) shows a highly coherent sequence of collisions.

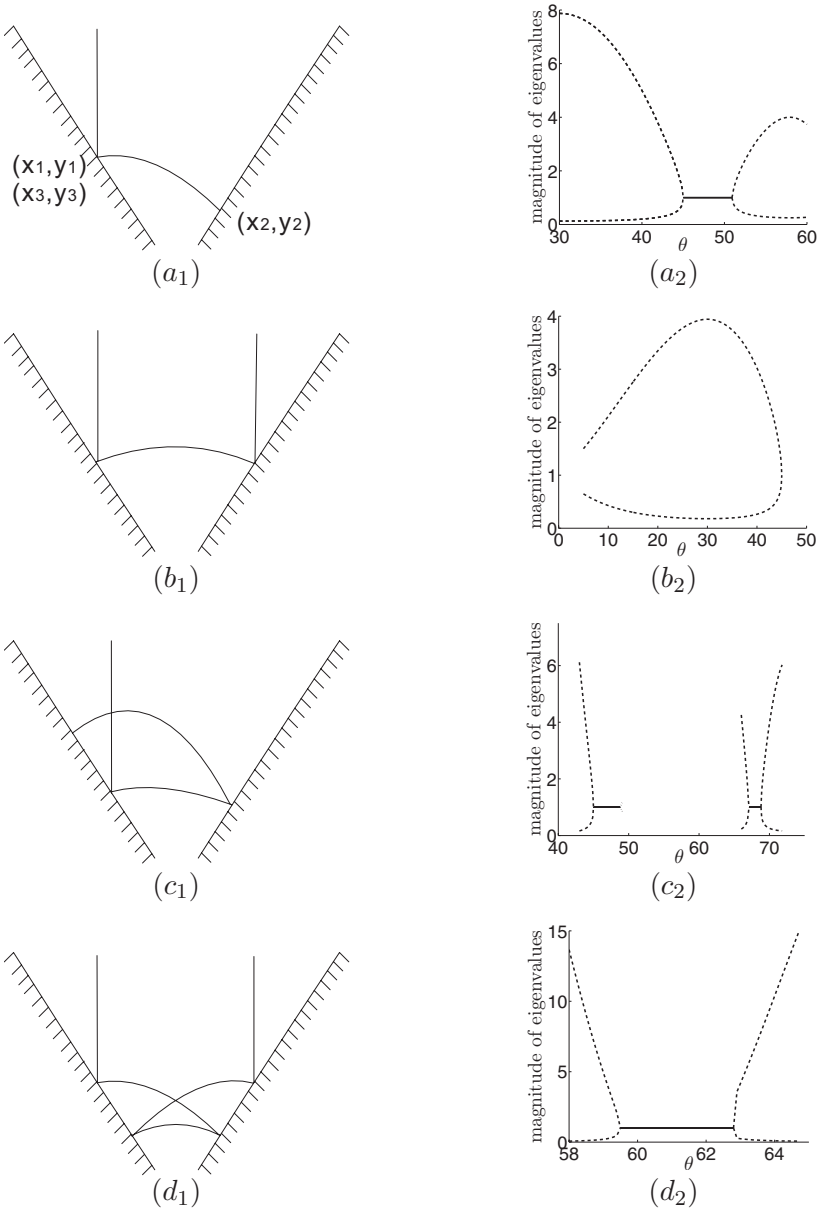

FIG. 7. The figures in the left column show the patterns of simple orbits for $e=1$. The figures in the right column show the corresponding magnitude of the eigenvalues of $\frac{\partial \mathbf{F}(\mathbf{v}_i)}{\partial \mathbf{v}_i}$. The solid curves indicate the range of θ for which the corresponding orbit is neutrally linearly stable. The dashed curves indicate the range of θ for which the corresponding orbit is neutrally unstable.

IV. PERIODIC ORBITS FOR $e=1$

Figures 2–6 showed clearly that the jumps are associated with the occurrence of repeated collision patterns. The closer e is to unity, the more pronounced the phenomenon is. This leads us to study funnels with $e=1$ and examine the periodic orbits in such systems. For a given angle θ, a number of periodic orbits are possible (see the left panel of Fig. 7 for the simplest few orbits). Each periodic orbit has a different sequence of collisions with the funnel walls. For a given collision sequence with m collisions, one needs to determine if the associated orbit can exist and whether it is stable. Let x_i and y_i be the location of the ith collision in the sequence and u_i and v_i be the x and y components of the particle velocity immediately before the ith collision. Since x_i and y_i are constrained to be on the funnel boundaries, we can eliminate x_i in favor of y_i. Furthermore, since the total energy is conserved, we can further eliminate y_i in favor of u_i and v_i. Hence the orbit is specified by the collision sequence and $\mathbf{v}_i=(u_i,v_i)^T$. Given $\mathbf{v}_i$ it is straightforward to calculate the locations and velocities immediately before the $(i+1)$th collision in the sequence. To compute $\mathbf{v}_{i+1}$ from $\mathbf{v}_i$, four different cases must be considered: $\mathbf{F}_{lr}$, $\mathbf{F}_{rl}$, $\mathbf{F}_{ll}$, and $\mathbf{F}_{rr}$. Here, $\mathbf{F}_{lr}$ represents the situation in which the ith collision is with the left wall and the $(i+1)$th collision is with the right wall. The symbols $\mathbf{F}_{rl}$, $\mathbf{F}_{ll}$, and $\mathbf{F}_{rr}$ are similarly defined. First, we consider the derivation of $\mathbf{F}_{lr}$. The velocity after the ith collision is

$$\begin{pmatrix} u_i' \\ v_i' \end{pmatrix} = \begin{pmatrix} \cos 2\theta & -\sin 2\theta \\ -\sin 2\theta & -\cos 2\theta \end{pmatrix} \begin{pmatrix} u_i \\ v_i \end{pmatrix}. \tag{1}$$

Due to energy conservation, we have $y_i=1+\frac{1}{2}d\tan\theta-\frac{1}{2}(u_i'^2+v_i'^2)$. Since the trajectory is composed of parabolic segments and each collision is constrained to coincide with the funnel walls, we have

$$y_i = -x_i \tan\theta \tag{2}$$

and

$$\frac{y_{i+1}}{x_{i+1}} = \frac{y_i + v_i' t_i - \frac{1}{2}t_i^2}{x_i + u_i' t_i} = \tan\theta. \tag{3}$$

This allows us to get the time between the two collisions:

$$t_i = -\sec\theta(u_i \sin 3\theta + v_i \cos 3\theta) + \sqrt{\sec^2\theta(u_i \sin 3\theta + v_i \cos 3\theta)^2 - 2(u_i^2 + v_i^2 - 2 - d\tan\theta)}.$$

The map from left wall to the right wall is thus given by

$$\mathbf{F}_{lr}: \quad \mathbf{v}_{i+1} = \begin{pmatrix} u_{i+1} \\ v_{i+1} \end{pmatrix} = \begin{pmatrix} u_i \cos 2\theta - v_i \sin 2\theta \\ -u_i \sin 2\theta - v_i \cos 2\theta - t_i \end{pmatrix}.$$

Second, we consider the derivation of $\mathbf{F}_{ll}$. For both $\mathbf{F}_{lr}$ and $\mathbf{F}_{ll}$, the ith collision is with the left wall. Therefore, Eqs. (1) and (2) still hold for $\mathbf{F}_{ll}$. However, for $\mathbf{F}_{ll}$, the $(i+1)$th collision is with the left wall and so Eq. (3) is replaced by

$$\frac{y_{i+1}}{x_{i+1}} = \frac{y_i + v_i' t_i - \frac{1}{2}t_i^2}{x_i + u_i' t_i} = -\tan\theta.$$

We can obtain the time between collisions $t_i = -2u_i \tan\theta - 2v_i$, and the map from left wall to the left wall is given by

$$\mathbf{F}_{ll}: \quad \mathbf{v}_{i+1} = \begin{pmatrix} u_{i+1} \\ v_{i+1} \end{pmatrix} = \begin{pmatrix} u_i \cos 2\theta - v_i \sin 2\theta \\ u_i(2\tan\theta - \sin 2\theta) + v_i(2 - \cos 2\theta) \end{pmatrix}.$$

The maps for $\mathbf{F}_{rl}$ and $\mathbf{F}_{rr}$ can be similarly constructed, and the results are

$$\mathbf{F}_{rl}: \quad \mathbf{v}_{i+1} = \begin{pmatrix} u_{i+1} \\ v_{i+1} \end{pmatrix} = \begin{pmatrix} u_i \cos 2\theta + v_i \sin 2\theta \\ u_i \sin 2\theta - v_i \cos 2\theta - t_i \end{pmatrix},$$

where

$$t_i = \sec\theta(u_i \sin 3\theta - v_i \cos 3\theta) + \sqrt{\sec^2\theta(u_i \sin 3\theta - v_i \cos 3\theta)^2 - 2(u_i^2 + v_i^2 - 2 - d\tan\theta)}$$

and

$$\mathbf{F}_{rr}: \quad \mathbf{v}_{i+1} = \begin{pmatrix} u_{i+1} \\ v_{i+1} \end{pmatrix} = \begin{pmatrix} u_i \cos 2\theta + v_i \sin 2\theta \\ u_i(\sin 2\theta - 2\tan\theta) + v_i(2 - \cos 2\theta) \end{pmatrix}.$$

Combining the effects of all m collisions we can therefore construct a two-dimensional map $\mathbf{F}$ defined by $\mathbf{v}_{i+m} = \mathbf{F}(\mathbf{v}_i)$. Since the orbit is periodic, we have $\mathbf{v}_i^* = \mathbf{F}(\mathbf{v}_i^*)$, where stars denote the periodic orbit. Here, we will show the calculation of the simplest periodic orbit [see Fig. 7(a1)]. The particle is released with zero velocity, so a simple calculation gives $u_1^* = 0$, $v_1^* = \sqrt{2(1 + \frac{d}{2}\tan\theta + x_1 \tan\theta)}$; then, it jumps from left wall to the right, so $\mathbf{v}_2^* = \mathbf{F}_{lr}(\mathbf{v}_1^*)$. In order to return along the same trajectory, the velocity before the second collision must be perpendicular to the wall, so $u_2^* = -v_2^* \tan\theta$. This allow us to compute the location of the first collision and velocities before this collision,

$$x_1^* = x_0^* = \frac{\left(1 + \frac{1}{2}d\tan\theta\right)(3 - \tan^2\theta)(5\tan^2\theta + 1)}{3\tan^5\theta - 18\tan^3\theta - 5\tan\theta},$$

$$y_1^* = -x_1^* \tan\theta,$$

$$u_1^* = 0, \quad v_1^* = -\sqrt{2\left(1 + \frac{1}{2}d\tan\theta + x_1^* \tan\theta\right)},$$

and also the location of the second collision and velocities before this collision are given by

$$x_2^* = x_1^* + 2v_1^{*2} \cos\theta \sin 3\theta, \quad y_2^* = x_2^* \tan\theta,$$

$$u_2^* = -v_1^* \sin 2\theta, \quad v_2^* = 2v_1^* \cos^2\theta.$$

For this orbit to exist, the locations of the collisions must be consistent with the funnel geometry which requires $|x_i| > d/2 - a\sin\theta$ for $i = 1, 2$. For $a \ll 1$ and $d \ll 1$ this can be reduced to $\frac{\pi}{6} + \frac{d}{4} - \frac{a}{8} < \theta < \frac{\pi}{3} - \frac{d}{4} + \frac{\sqrt{3}a}{8}$. Other orbits shown in Fig. 7 can be constructed in the same way.

Not all orbits are stable. Unstable periodic orbits cannot be observed since any small disturbance will eventually destroy the periodicity. Adding a small perturbation $\delta\mathbf{v}_i$ in $\mathbf{v}_i$ yields $\delta\mathbf{v}_{i+m} = \frac{d\mathbf{F}}{d\mathbf{v}_i}\big|_{\mathbf{v}_i = \mathbf{v}_i^*} \delta\mathbf{v}_i$. Since the process is nondissipative, the map $\mathbf{F}$ must preserve area in the phase space and so the 2-by-2 matrix $\frac{d\mathbf{F}}{d\mathbf{v}_i}\big|_{\mathbf{v}_i = \mathbf{v}_i^*}$ must have unit determinant. Therefore the characteristic polynomial of the matrix is given by $\lambda^2 - \mathrm{tr}(\frac{d\mathbf{F}}{d\mathbf{v}_i}\big|_{\mathbf{v}_i = \mathbf{v}_i^*})\lambda + 1 = 0$. If $|\mathrm{tr}(\frac{d\mathbf{F}}{d\mathbf{v}_i}\big|_{\mathbf{v}_i = \mathbf{v}_i^*})| < 2$, the orbit will be linearly neutrally stable. This means that trajectories that start sufficiently close to the periodic orbit will neither approach nor diverge from the periodic orbit while maintaining the same collision sequence. If $|\mathrm{tr}(\frac{d\mathbf{F}}{d\mathbf{v}_i}\big|_{\mathbf{v}_i = \mathbf{v}_i^*})| \geq 2$, then the orbit will be linearly unstable. In this case, trajectories that start close to the periodic orbit will diverge from the periodic orbit until the particle can no longer follow the given collision sequence. At this point the dynamics becomes complicated and the trajectories can become highly sensitive to initial conditions.

Below we derive the stability limits for the simplest orbit shown in Fig. 7(a1). Given the collision sequence for this orbit, we have $\mathbf{v}_2 = \mathbf{F}_{lr}(\mathbf{v}_1)$, $\mathbf{v}_3 = \mathbf{F}_{rl}(\mathbf{v}_2)$, and $\mathbf{v}_4 = \mathbf{F}_{ll}(\mathbf{v}_3)$. Using the chain rule, we have

$$\left.\frac{d\mathbf{F}}{d\mathbf{v}_1}\right|_{\mathbf{v}_1=\mathbf{v}_1^*} = \left.\frac{d\mathbf{F}_{ll}}{d\mathbf{v}_3}\right|_{\mathbf{v}_3=\mathbf{v}_3^*} \cdot \left.\frac{d\mathbf{F}_{rl}}{d\mathbf{v}_2}\right|_{\mathbf{v}_2=\mathbf{v}_2^*} \cdot \left.\frac{d\mathbf{F}_{lr}}{d\mathbf{v}_1}\right|_{\mathbf{v}_1=\mathbf{v}_1^*}. \quad (4)$$

Using the maps given above, we obtain

$$\frac{d\mathbf{F}_{lr}}{d\mathbf{v}_1} = \begin{pmatrix} \frac{\partial u_2}{\partial u_1} & \frac{\partial u_2}{\partial v_1} \\ \frac{\partial v_2}{\partial u_1} & \frac{\partial v_2}{\partial v_1} \end{pmatrix} = \begin{pmatrix} \cos 2\theta & -\sin 2\theta \\ -\sin 2\theta - \frac{\partial t_1}{\partial u_1} & -\cos 2\theta - \frac{\partial t_1}{\partial v_1} \end{pmatrix},$$

where

$$\frac{\partial t_1}{\partial u_1} = -\sec\theta \sin 3\theta + \frac{\sec^2\theta \sin 3\theta(u_1 \sin 3\theta + v_1 \cos 3\theta) - 2u_1}{\sqrt{\sec^2\theta(u_1 \sin 3\theta + v_1 \cos 3\theta)^2 - 2(u_1^2 + v_1^2 - 2 - d\tan\theta)}},$$

$$\frac{\partial t_1}{\partial v_1} = -\sec\theta \cos 3\theta + \frac{\sec^2\theta \cos 3\theta(u_1 \sin 3\theta + v_1 \cos 3\theta) - 2v_1}{\sqrt{\sec^2\theta(u_1 \sin 3\theta + v_1 \cos 3\theta)^2 - 2(u_1^2 + v_1^2 - 2 - d\tan\theta)}}.$$

Substituting $\mathbf{v}_1^*$ for $\mathbf{v}_1$, we obtain:

$$\left.\frac{d\mathbf{F}_{lr}}{d\mathbf{v}_1}\right|_{\mathbf{v}_1=\mathbf{v}_1^*} = \begin{pmatrix} \cos 2\theta & -\sin 2\theta \\ \tan\theta\left(8\cos^4\theta - 6\cos^2\theta + \frac{1}{2}\right) & 8\cos^4\theta - 10\cos^2\theta + \frac{3}{2} \end{pmatrix}.$$

Similarly, we get

$$\left.\frac{d\mathbf{F}_{rl}}{d\mathbf{v}_2}\right|_{\mathbf{v}_2=\mathbf{v}_2^*} = \begin{pmatrix} \cos 2\theta & \sin 2\theta \\ -\tan\theta(16\cos^4\theta - 14\cos^2\theta + 1) & 16\cos^4\theta - 22\cos^2\theta + 4 \end{pmatrix}$$

and

$$\left.\frac{d\mathbf{F}_{ll}}{d\mathbf{v}_3}\right|_{\mathbf{v}_3=\mathbf{v}_3^*} = \begin{pmatrix} \frac{\partial u_4}{\partial u_3} & \frac{\partial u_4}{\partial v_3} \\ \frac{\partial v_4}{\partial u_3} & \frac{\partial v_4}{\partial v_3} \end{pmatrix} = \begin{pmatrix} \cos 2\theta & -\sin 2\theta \\ 2\tan\theta - \sin 2\theta & 2 - \cos 2\theta \end{pmatrix}.$$

Combining these results, (4) becomes

$$\begin{pmatrix} a_{11} & a_{12} \\ a_{21} & a_{22} \end{pmatrix},$$

where

$$a_{11} = 256\cos^{10}\theta - 896\cos^8\theta + 1120\cos^6\theta - 600\cos^4\theta + 129\cos^2\theta - 8,$$

$$a_{12} = -\tan\theta(256\cos^{10}\theta - 768\cos^8\theta + 736\cos^6\theta - 240\cos^4\theta + 21\cos^2\theta),$$

$$a_{21} = -\tan\theta(256\cos^{10}\theta - 1024\cos^8\theta + 1440\cos^6\theta - 848\cos^4\theta + 197\cos^2\theta - 13),$$

$$a_{22} = -256\cos^{10}\theta + 1152\cos^8\theta - 1888\cos^6\theta + 1352\cos^4\theta - 393\cos^2\theta + 34.$$

The orbit will be linearly neutrally stable if $|\mathrm{tr}(\left.\frac{d\mathbf{F}}{d\mathbf{v}_1}\right|_{\mathbf{v}_1=\mathbf{v}_1^*})| < 2$, which gives

$$|256\cos^8\theta - 768\cos^6\theta + 752\cos^4\theta - 264\cos^2\theta + 26| < 2.$$

We can therefore obtain the range of θ in which this orbit exists and is linearly neutrally stable, as $\theta \in (\frac{\pi}{4}, \arccos\sqrt{\frac{3-\sqrt{2}}{4}}) = (45°, 50.97°)$. Similar computations can be performed for other orbits.

In the right panel of Fig. 7 we plot the magnitudes of the eigenvalues as a function of the funnel angle for the corresponding periodic orbits shown on the same row in the left panel. The ranges of θ for which each orbit is linearly neutrally stable are shown as solid curves while the unstable ranges of θ are shown as dotted curves. In particular, Fig. 7(b2) shows that the orbit shown in Fig. 7(b1) is unstable for all values of θ. The neutrally stable ranges are also marked in Fig. 2, and one can clearly see that these ranges correspond exactly with the ranges in which the inelastic particle stays in the funnel for an unexpectedly long time. Moreover, the sensitivity of the trajectories to initial conditions is strongly correlated with the stability of the associated periodic orbits.

In order to understand the extent to which the behavior of elastic particles is dominated by periodic orbits, we have performed simulations with an elastic particle in which we record the x locations of the first 2000 collisions for a given

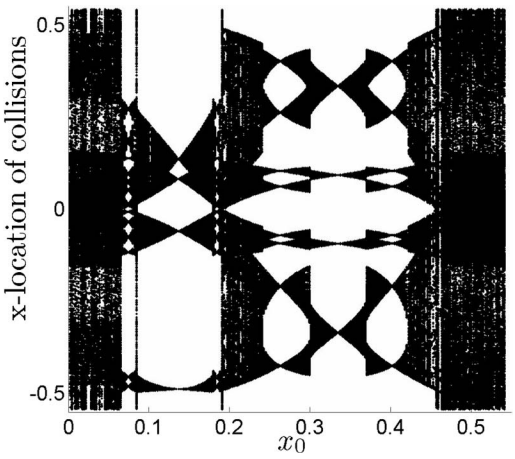

FIG. 8. The x locations of the first 2000 collisions are plotted as a function of the input location x_0 for $\theta=61°$ and $e=1$. The input locations for which trajectories stay close to periodic orbits are clearly visible. In the similar plot at $\theta=59°$, the points marking collision locations fill the entire space. This confirms that trajectories that stay close to periodic orbits do not occur.

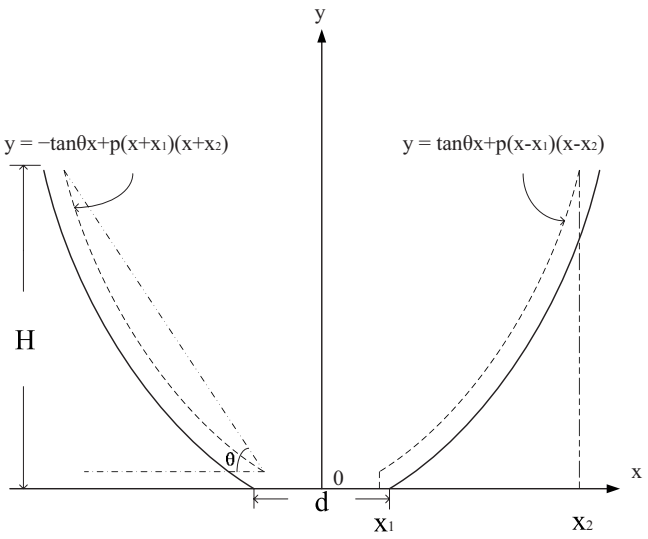

FIG. 9. A schematic for a system with parabolic walls. The dotted curves are the curves that the center of the ball collides with, and the solid curves are the boundaries of the funnel.

input location. In Fig. 8 we plot the results as a function of input location for $\theta=61°$. There are a number of periodic orbits, and the periodic orbit shown in Fig. 7(d2) can be seen for x_0 approximately 0.33. The trajectories of particles that have input locations in the range (0.3, 0.37) stay close to this periodic orbit. Other orbits are also visible, for example, an orbit with eight collisions can be seen for x_0 approximately 0.27 and trajectories of particles that have input locations in the range (0.24, 0.3) stay close to this orbit. However, there are other regions such as (0, 0.7) and (0.47, 0.53) in which no clear pattern exists. For $\theta=59°$, the results are dramatically different. In this case, there are no clear periodic orbits and the points denoting the collision locations fill the entire space in the figure. Therefore we do not present this figure.

V. THEORETICAL EXPLANATION

Now we provide an explanation of the jumps that occur in Figs. 2–4. For $e<1$ periodic orbits do not exist. Nevertheless, the particle trajectories can adopt the same collision sequence as the corresponding elastic particle ($e=1$) until near the time when the particle exits the funnel. We will refer to these trajectories as quasiperiodic orbits. The jumps are the remnants of the neutrally stable periodic orbits shown in the left panel of Fig. 7. Periodic orbits exist for wide ranges of the funnel angle θ, but it is not the existence of periodic orbits that leads to the large jumps in the mean duration, impulse, and energy loss. Rather, it is the existence of neutrally stable periodic orbits that leads to the anomalous behavior.

The labels on Fig. 2 allow one to easily identify each jump with the associated orbit in Fig. 7. The simpler an orbit is, the larger the jump associated with it is. This is because the locations of the collisions in simple orbits tend to be relatively far away from the exit. The quasiperiodic orbit therefore takes a relatively long time for the collision locations to move down toward the exit. On the other hand, complicated orbits tend to have a collision whose location is relatively near to the exit. Therefore the particle will exit the funnel much earlier than simple trajectories. This is why the major jumps in Figs. 2–4 can be determined by considering the simplest few orbits. The jumps associated with more complicated orbits have a relatively weak effect. As e gets smaller, particles lose more energy per collision and the collision locations move down toward the exit more quickly. Consequently, even the simple orbits will stay a relatively short time in the funnel. Therefore the jumps become less pronounced as e decreases.

Finally, we discuss the effects of the gap size. Our numerical simulations show that as one increases the gap size the overall shapes of the curves for duration are very similar to those shown in Figs. 2–4. For the average duration, the average impulse, and the average energy loss, the curves are shifted downwards as the gap size increases. The size of the jumps decreases, but the locations of the jumps remains the same. The reduction in jump size is larger for jumps associated with more complicated orbits. This behavior can be easily understood by considering the effects of gap width on the existence of stable orbits.

So far, all our theoretical and numerical studies have focused on the anomalous phenomenon that occurs when a perfectly circular particle falls through a funnel with flat surfaces. That is, a particle may take a longer time to fall through a funnel with steeper walls than a funnel with less steep walls. It is natural to ask whether the anomalous phenomenon still exits when the system deviates from this perfect setting. To demonstrate that this phenomenon indeed exists, we first consider a perfectly circular particle falling through a funnel whose walls are not flat. We consider walls that have a shape chosen such that when the ball collides with the walls, its center of mass lies on a parabola (see Fig. 9) given by $y=-\tan\theta x+p(x+x_1)(x+x_2)$ for $-x_2\leq x\leq -x_1$ and $y=\tan\theta x+p(x-x_1)(x-x_2)$ for $x_1\leq x\leq x_2$, where $x_1=\frac{d}{2}$

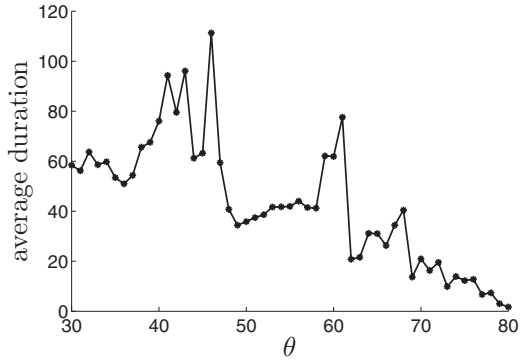

FIG. 10. The average duration is plotted against θ for systems with concave parabolic walls (similar to Fig. 9). Here, $e=0.99$, $d=0.04$, and $p=-0.2$

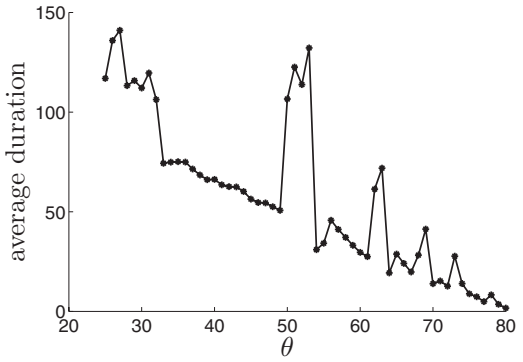

FIG. 11. The average duration is plotted against θ for systems with convex parabolic walls (see Fig. 9). Here, $e=0.99$, $d=0.04$, and $p=0.2$

$-a \sin\theta$ and $x_2=\frac{d}{2}+H\cot\theta-\frac{a}{\sin\theta}$. The opening of the funnel is located at $-\frac{d}{2}\leq x\leq\frac{d}{2}$ and $y=0$. The parameter θ that appears in the above equations is defined as the effective declining angle of the funnel (see Fig. 9). In Fig. 10, we plot the average duration that a particle stays inside the funnel with concave parabolic walls ($p=-0.2$) as a function of θ. In Fig. 11, we plot the average duration for a funnel with convex parabolic walls ($p=0.2$). Figures 10 and 11 clearly show that the anomalous behavior still exists for funnels with walls of parabolic shape. All large jumps that were present for the case of flat walls are still present in the case of both concave and convex parabolic walls. Furthermore, Fig. 11 shows an additional anomalous peak near $\theta=28°$, which does not exist in the case of flat walls. This peak is related to the periodic orbit shown in Fig. 7(b1), which was unstable for flat walls, but becomes stable for convex parabolic walls.

To demonstrate that the anomalous phenomenon is not a singular behavior of perfectly circular particles, we consider particles with elliptic shape falling through a funnel with parabolic walls; the shapes of walls are given by $y=-\tan\theta(x+\frac{d}{2})+p(x+\frac{d}{2})(x+\frac{d}{2}+H\cot)$ for $-(\frac{d}{2}+H\cot)\leq x\leq-\frac{d}{2}$ and $y=\tan\theta(x-\frac{d}{2})+p(x-\frac{d}{2})[x-(\frac{d}{2}+H\cot)]$ for $\frac{d}{2}\leq x\leq\frac{d}{2}+H\cot$. The opening of the funnel is located at $-\frac{d}{2}\leq x\leq\frac{d}{2}$ and $y=0$. When an elliptic-shaped particle collides with the walls, the collisional impulse, in general, does not pass through the center of mass of the particle and an instantaneous impulsive torque is exerted on the particle. This causes the particle to rotate.

We performed simulations with long and short axes of the elliptic particles equal to 0.0202 and 0.02, respectively. However, numerical simulations for an elliptic particle falling through a parabolic funnel are much more time consuming than that for a circular particle falling through a parabolic funnel. This is due to the complexity in determining the collision points for elliptic particles. However, all that is required to verify the existence of anomalous behavior is to perform simulations with two systems with different θ and demonstrate that the system with smaller θ has larger average duration than the system with larger θ. We consider the case of flat walls ($p=0$) with $\theta=44°$ and $\theta=46°$ (these angles are those that give large jumps in the case of circular particles; see Fig. 2). For $\theta=44°$ the average duration is 45.64 and for $\theta=46°$ the average duration is 91.32. We also considered elliptic particles falling through a funnel with concave parabolic walls ($p=-0.2$) with $\theta=36°$ and $\theta=41°$ (as suggested by Fig. 10). For $\theta=36°$ the average duration is 38.51 and for $\theta=41°$ the average duration is 55.59. Similarly, we also considered elliptic particles falling through a funnel with convex parabolic walls ($p=0.2$) with $\theta=45°$ and $\theta=52°$ (as suggested by Fig. 11). For $\theta=45°$ the average duration is 29.73 and for $\theta=52°$ the average duration is 78.22. Therefore we have demonstrated the anomalous behavior presented in a system of perfectly circular particles falling through a funnel with flat walls can also occur in a considerably larger class of systems.

In conclusion, we have studied the simple system of an inelastic particle falling through a funnel. Counterintuitively, an increase in the steepness of the funnel walls can lead the particle to stay longer in the funnel, exert a larger total impulsive force on the funnel walls, and lose more energy. Our theoretical analysis shows that these phenomena are due to the existence of neutrally stable quasiperiodic orbits.

ACKNOWLEDGMENT

The work described in this paper was fully supported by the Research Grants Council of Hong Kong, Special Administrative Region, China, Project No. CityU 103205.

[1] K.-L. Schick and A. A. Verveen, Nature (London) **251**, 599 (1974).

[2] G. W. Baxter, R. P. Behringer, T. Fagert, and G. A. Johnson, Phys. Rev. Lett. **62**, 2825 (1989).

[3] X-l. Wu, K. J. Maloy, A. Hansen, M. Ammi, and D. Bideau, Phys. Rev. Lett. **71**, 1363 (1993).

[4] C. T. Veje and P. Dimon, Phys. Rev. E **54**, 4329 (1996).

[5] C. T. Veje and P. Dimon, Phys. Rev. E **56**, 4376 (1997).

[6] O. Moriyama, N. Kuroiwa, M. Matsushita, and H. Hayakawa, Phys. Rev. Lett. **80**, 2833 (1998).
[7] T. Le Pennec, M. Ammi, J. C. Messager, and A. Valance, Eur. Phys. J. B **7**, 657 (1999).
[8] E. Longhi, N. Easwar, and N. Menon, Phys. Rev. Lett. **89**, 045501 (2002).
[9] S. Horlück, M. van Hecke, and P. Dimon, Phys. Rev. E **67**, 021304 (2003).
[10] D. Helbing, A. Johansson, J. Mathiesen, M. H. Jensen, and A. Hansen, Phys. Rev. Lett. **97**, 168001 (2006).
[11] See, for example, the special issue Chaos **9** (3) (1999) devoted to granular materials.
[12] A. Mehta and J. M. Luck, Phys. Rev. Lett. **65**, 393 (1990).
[13] J. M. Luck and A. Mehta, Phys. Rev. E **48**, 3988 (1993).
[14] S. McNamara and W. R. Young, Phys. Fluids A **4**, 496 (1992).
[15] J. J. Wylie and Q. Zhang, Phys. Rev. E **74**, 011305 (2006).